

General parametrization for energy density of quintessence field

Shiriny Akthar and Md. Wali Hossain^{ID}

Department of Physics, Jamia Millia Islamia,
New Delhi, 110025, India

E-mail: shirinyakthar@gmail.com, mhossain@jmi.ac.in

Abstract. We present a general parametrization for energy density of a quintessence field, a minimally coupled canonical scalar field which rolls down slowly during the late time. This parametrization can mimic all classes of quintessence dynamics, namely scaling-freezing, tracker and thawing dynamics for any redshift. For thawing dynamics the parametrization needs two free parameters while for scaling-freezing and tracker dynamics it needs at least four free parameters. More parameters make the model less interesting from the observational data analysis point of view but as we expect more precise data in future it may be possible to constrain the models with multiple free parameters which can tell about the dynamics more precisely. One of the main advantage of this parametrization is that it reduces the computational time to significant amount while mimicking the actual scalar field dynamics for all redshifts which may not be possible with other existing parametrizations. We compare the parametrization with two and four parameters with the standard Λ CDM model using cosmological observational data from Planck 2018 (distance priors), DESI 2024 DR1, PantheonPlus, Hubble parameter measurements and the redshift space distortion. We find that the observational data prefers standard Λ CDM model over other models. If we allow phantom region then it is more preferred by the data compared to non-phantom thawing quintessence. Also, we can not strictly comment on the preference on the dynamical dark energy over a cosmological constant as claimed by the DESI 2024 DR1 results.

Contents

1	Introduction	1
2	Background equations	3
3	Scalar field dynamics and the parametrization	4
4	Scaling-freezing dynamics	6
5	Tracker dynamics	10
6	Thawing dynamics	12
7	Observational Constraints	14
7.1	Observational data	15
7.1.1	CMB	15
7.1.2	BAO data from DESI DR1	15
7.1.3	Type-Ia Supernova	15
7.1.4	Observational Hubble Data	15
7.1.5	Redshift Space Distortion	15
7.2	Results	16
8	Discussions and Conclusions	19

1 Introduction

After Planck 2013 results [1] the almost cosmological constant (CC) appeared not only as the most favoured but the sufficient candidate as the dark energy with constant equation of state (EoS) to explain the late time universe. So, the relevance of dynamical dark energy (DDE) [2, 3] was almost became irrelevant. It is very recently, after the local measurement of the present value of the Hubble constant (H_0) by the SH0ES team [4], which observed $\sim 5\sigma$ tension between the local measurement of H_0 and the constraint coming from cosmic microwave background (CMB) observations assuming the standard Λ CDM model [5], the DDE becomes important. Apart from the Hubble tension [6–9] the standard Λ CDM model is also in tension in the measurements of growth rate known as the $S_8 = \sigma_8 \sqrt{\Omega_{m0}/0.3}$ tension [10, 11], where σ_8 is the standard deviation of matter density fluctuations at present for linear perturbation in spheres of radius $8h^{-1}\text{Mpc}$ and Ω_{m0} is the present value of matter density parameter. On top of these tensions the measurements of baryon acoustic oscillation (BAO) by the DESI experiment in 2024 shows a preference on DDE over CC [12–23]. So, it's a high time to study DDE.

One of the simplest candidate of DDE is the minimally coupled canonical scalar field, ϕ . If this scalar field rolls slowly during the late time we call it a quintessence field [24–26] which can explain the late time acceleration [2]. In a cosmological background, the scalar field EoS w_ϕ varies between -1 to 1 . $w_\phi = -1$ signifies potential energy domination while $w_\phi = 1$ signifies kinetic energy domination. The energy density of the scalar field ρ_ϕ can be represented as $\rho_\phi \sim e^{-3\int(1+w_\phi)d\ln a}$. $w_\phi = -1$ gives constant ρ_ϕ and it varies as a^{-6} for

$w_\phi = 1$. Thus, we can expect wide variation in the scalar field dynamics in a cosmological background. In fact, we can classify the dynamics in three classes, namely, scaling-freezing [27–29], tracker [30, 31] and thawing [32] models. Because of the large Hubble damping coming from the background energy density in the scaling-freezing and tracker dynamics the scalar field is frozen in the past. During the frozen period the ρ_ϕ increases and when it becomes comparable to the background the scalar field again starts rolling down the potential. Depending upon the nature of the potential the scalar field energy density can either scale the background energy density (for scaling-freezing) or decay a little slower than the background energy density (for tracker). For tracker, since the decay of scalar field energy density is slower than the background the scalar field eventually takes over matter during the recent past which may give rise to late time acceleration with viable cosmology [33]. For scaling-freezing the scalar field scales the background after the frozen period and then takes over matter in the recent past [28] which can be achieved either by having a sufficiently shallow region in the potential during the late time or by having a nonminimal coupling between the scalar field and matter in the Einstein frame. For both the dynamics the late time dynamics is an attractor solution. On the other hand the thawing dynamics is very sensitive to the initial conditions. In this dynamics the scalar field is frozen from the past behaving like a CC which starts to thaw from the recent past giving rise to deviation from CC [32].

While scalar field gives interesting dynamics in the cosmological background it can be very expensive computationally while running simulations to analyse cosmological data. For this reason it is always helpful to work with parametrized form of EoS or energy density of the DDE. In this regard the Chevallier-Polarski-Linder (CPL) [34, 35] parametrization of EoS of DDE works very well for low redshifts with only two parameters and this is the most widely used parametrization. Apart from the CPL parametrization many other parametrization have been studied in the literature *e.g.*, logarithmic (Efstathiou model) [36], Jassal-Bagla-Padmanabhan [37], Barboza-Alcaniz [38] parametrization. Generally these parametrizations can mimic DDE at very low redshifts. Now, introduction of scalar field gives actual model of DDE which can have some specific nature in dynamics and may not be mimicked by any arbitrary parametrization specially at higher redshifts. So, in this paper, we present a general parametrization of the energy density of quintessence field which not only can mimic the cosmological dynamics of a quintessence field for a particular potential but also can be considered as a model-agnostic framework for studying dynamical dark energy. This enables us to explore a broad class of quintessence models with or without assuming specific forms of the scalar field potential.

The main challenge for this general parametrization is to reduce the number of free parameters. In this regard, we have deduced some relations to reduce the number of free parameters. The thawing dynamics can be represented with two free parameters while the scaling-freezing and tracker dynamics can be represented with at least four parameters. Now, having more parameters makes the scenario less interesting from the data analysis point of view but these parameters are needed if we are interested specifically in the scalar field dynamics. We expect that in near future we will have more precise data which can constrain these parameters and we will be able to tell about the scalar field dynamics more precisely. Also, working with the scalar fields can make the computation, for data analysis, very expensive in time. This general parametrization reduces the computational time to significant amount while preserving the actual scalar field dynamics for a particular potential for any redshift. This is one of the main advantage of this parametrization.

The paper is organised as follows. In Sec. 2 we introduce the background cosmologi-

cal equations including scalar field equation of motion. In Sec. 3 we introduce the general parametrization of the energy density of a quintessence field. The scaling-freezing dynamics has been studied in Sec. 4. The tracker dynamics has been studied in Sec. 5 while in Sec. 6. The study of observational constraints has been done in Sec. 7. We summarise and conclude our results in Sec. 8.

2 Background equations

We consider a minimally coupled canonical scalar field with the following action

$$\mathcal{S} = \int d^4x \sqrt{-g} \left[\frac{M_{\text{Pl}}^2}{2} R - \frac{1}{2} \partial_\mu \phi \partial^\mu \phi - V(\phi) \right] + \mathcal{S}_m + \mathcal{S}_r, \quad (2.1)$$

where $M_{\text{Pl}} = 1/\sqrt{8\pi G}$ is the reduced Planck mass and $V(\phi)$ is the potential of the field. \mathcal{S}_r and \mathcal{S}_m are the actions for radiation and matter respectively.

Varying the action (2.1) with respect to (w.r.t.) the metric $g_{\mu\nu}$ gives the Einstein's field equation

$$M_{\text{Pl}}^2 G_{\mu\nu} = T_{(m)\mu\nu} + T_{(r)\mu\nu} + T_{(\phi)\mu\nu}, \quad (2.2)$$

where

$$T_{(\phi)\mu\nu} = \phi_{;\mu} \phi_{;\nu} - \frac{1}{2} g_{\mu\nu} (\nabla\phi)^2 - g_{\mu\nu} V(\phi). \quad (2.3)$$

The equation of motion of the scalar field can be calculated by varying the action (2.1) w.r.t. the scalar field ϕ and it is given by

$$\square\phi - V_\phi(\phi) = 0, \quad (2.4)$$

where subscript ϕ denotes the derivative wrt ϕ .

In flat Friedmann–Lemaître–Robertson–Walker (FLRW) metric, given by

$$ds^2 = -dt^2 + a(t)^2 \delta_{ij} dx^i dx^j, \quad (2.5)$$

where $a(t)$ is the scale factor, the Friedman equations are given by

$$3H^2 M_{\text{Pl}}^2 = \rho_m + \rho_r + \frac{1}{2} \dot{\phi}^2 + V(\phi) \quad (2.6)$$

$$(2\dot{H} + 3H^2) M_{\text{Pl}}^2 = -\frac{1}{3} \rho_r - \frac{1}{2} \dot{\phi}^2 + V(\phi). \quad (2.7)$$

The equation of motion of the scalar field is given by

$$\ddot{\phi} + 3H\dot{\phi} + \frac{dV}{d\phi} = 0. \quad (2.8)$$

Effective equation of state (EoS) and the EoS of the scalar field are given by

$$w_{\text{eff}} = - \left(1 + \frac{2}{3} \frac{\dot{H}}{H^2} \right), \quad (2.9)$$

$$w_\phi = \frac{\frac{1}{2}\dot{\phi}^2 - V(\phi)}{\frac{1}{2}\dot{\phi}^2 + V(\phi)}. \quad (2.10)$$

We define the following two functions

$$\lambda = -M_{\text{Pl}} \frac{V'(\phi)}{V}, \quad (2.11)$$

$$\Gamma = \frac{V''(\phi)V(\phi)}{V'(\phi)^2}. \quad (2.12)$$

While the function λ signifies the slope of the potential the function Γ represents the nature of the potential, *e.g.*, $\Gamma = 1$ for an exponential potential of constant slope λ . The nature of these functions determines the scalar field dynamics [3, 33].

3 Scalar field dynamics and the parametrization

Scalar field dynamics depends on the potential $V(\phi)$. More specifically it depends on the nature of the functions λ and Γ . Considering different kinds of scalar field dynamics we can classify them in three categories, (i) scaling-freezing [2, 27], (ii) tracking [30, 31] and (iii) thawing dynamics [32, 39]. (i) The scaling-freezing dynamics can be achieved in potentials with large slope λ while Γ should be equal or very close to 1 for some region of the potential with large slope where the scalar field energy density will scale the background energy density. In this dynamics the scalar field remains frozen in the past, just before reaching the scaling solution, due to large Hubble damping and then scale the background during the intermediate time before taking over matter giving rise to late time acceleration. In this dynamics λ should vary from a large value to a smaller value to achieve viable cosmology. If λ remains constant and large then for $\Gamma = 1$ we have only scaling solutions where the scalar field will scale the background forever and can not take over it [27]. (ii) Like the scaling-freezing dynamics in tracker dynamics also we need large slope of the potential but $\Gamma > 1$ [31] with a frozen stage of the scalar field in the past just before reaching the tracker behaviour. As Γ goes away from 1 towards the larger value, for large slope λ , the scalar field does not scale the background exactly but decays a little slower than background which results an eventual domination of scalar field during the late time which may give rise to late time acceleration. The advantage of both scaling-freezing and tracking dynamics is that the late time cosmology is an attractor solution can be similar for an wide range of initial conditions. The disadvantage is that the requirements of specific nature of the functions λ and Γ put a constraint on the nature of the potential and not all potential can give rise to these dynamics. (iii) In thawing dynamics the scalar field remains frozen until it starts evolving slowly from the recent past giving rise to late time acceleration. In this dynamics the scalar field behaves like a CC for most of the time except very recently when it starts evolving and deviates from the CC nature. To have viable cosmology the scalar field can not deviate much from the CC at present which can be achieved by tuning the initial conditions. So, this dynamics is very initial condition dependent but can be achieved for any potential. As the scalar field remains frozen for most of the time and then evolves slowly the scalar field dynamics may not capture the actual interesting features of the potential in this dynamics at least until the present time.

Considering the above mentioned dynamics of a scalar field in the flat cosmological background we introduce the following parametrization of the scalar field energy density

$$\rho_\phi(z) = \sum_{i=1}^f \frac{\rho_{0i}}{1 + \left(\frac{1+z_i}{1+z}\right)^{\alpha_i}} + \rho_{\text{KE}} (1+z)^6. \quad (3.1)$$

ρ_{KE} sets the initial value of ρ_ϕ . $\rho_{\text{KE}} = 0$ implies that the scalar field is initially frozen *i.e.*, its kinetic term is almost zero. If $\rho_{\text{KE}} \neq 0$ then ρ_ϕ initially falls as a^{-6} and becomes subdominant and because of the Hubble damping the scalar field freezes to evolve. During the frozen period ρ_ϕ increases and becomes comparable to the background energy density and starts evolving again. f is the number of frozen periods in the scalar field dynamics which will depend on the nature of the scalar field dynamics governed by the nature of the potential, more precisely the nature and the values of the functions λ and Γ . So, $f = 1$ is the first frozen period of the scalar field in the past. ρ_{0i} 's and z_i 's are constants. Even though we may need more than one z_i but all the z_i 's, for $i > 1$, can be represented in terms of $z_{i=1}$ and ρ_{0i} 's using the following relation

$$1 + z_{i>1} = \left(\frac{2\rho_{0(i-1)}}{\rho_{0i}} - 1 \right)^{-1/\alpha_{i-1}} (1 + z_{i-1}). \quad (3.2)$$

The Hubble parameter is given by the Friedmann equation

$$3H^2(z)M_{\text{Pl}}^2 = \rho_{\text{m}}(z) + \rho_{\text{r}}(z) + \rho_\phi(z), \quad (3.3)$$

Since the total density parameter should be one, at $z = 0$, we have the constraint equation

$$\Omega_{\text{m}0} + \Omega_{\text{r}0} + \sum_{i=1}^f \frac{\Omega_{0i}}{1 + (1 + z_i)^{\alpha_i}} + \Omega_{\text{KE}} = 1 \quad (3.4)$$

which reduces one more free parameter. In the last equation we have considered $\Omega_\phi \rightarrow \rho_\phi/\rho_{\text{c}0}$, *i.e.*, $\Omega_{0i} \rightarrow \rho_{0i}/\rho_{\text{c}0}$ and $\Omega_{\text{KE}} \rightarrow \rho_{\text{KE}}/\rho_{\text{c}0}$. Also, ρ_{KE} fixes the initial energy density of the scalar field and should be very small and it is sufficient to fix the value of Ω_{KE} and not consider it as a model parameter as it will have almost no effect on the late time evolution of the scalar field energy density. So, the constraint equation becomes

$$\Omega_{\text{m}0} + \Omega_{\text{r}0} + \sum_{i=1}^f \frac{\Omega_{0i}}{1 + (1 + z_i)^{\alpha_i}} = 1 \quad (3.5)$$

Now, practically, at $z = 0$, the dominant contribution will come from the $i = f$ term as long as z_{f-1} is not very close to 0. This gives us

$$\Omega_{\text{m}0} + \Omega_{\text{r}0} + \frac{\Omega_{0f}}{1 + (1 + z_f)^{\alpha_f}} = 1. \quad (3.6)$$

The above equation gives us

$$1 + z_f = \left(\frac{\Omega_{0f}}{1 - \Omega_{\text{m}0} - \Omega_{\text{r}0}} - 1 \right)^{1/\alpha_f}, \quad \text{for } \alpha_f \neq 0. \quad (3.7)$$

Using the above equation we can see from Eq. (3.2) that all the z_{0i} 's can be represented by ρ_{0i} 's which reduces one more free parameter. This will be clearer in the forthcoming sections where we give explicit examples of scalar field dynamics and how the parametrization (3.1) can reproduce the behaviour of the scalar field dynamics. So, finally, we have only ρ_{0i} 's as the free parameters in the parametrization (3.1). In the next sections, we will see that the maximum value of i , *i.e.*, $i_{\max} \leq 2$ is sufficient to represent the scalar field dynamics. So, we can represent scalar field dynamics with at most 4 additional parameters, two for ρ_{0i} 's and two for α_i 's. Eq. (3.6) may not be valid when z_{f-1} is very close to 0. This can happen when the kinetic energy of the scalar field still contributes significantly even at present. This scenario can particularly be observed for tracker dynamics in some potentials such as the inverse power law potential [24, 30] which does not produce a viable cosmology [30, 33]. The inverse axionlike potential gives rise to viable cosmology along with tracker dynamics [33]. For this case the potential energy dominates from the recent past and we can use Eq. (3.6) safely. We shall discuss this in details in Sec. 5

When $\alpha_f = 0$ we have $\Omega_{0f} = 2(1 - \Omega_{m0} - \Omega_{r0})$ using which we can have

$$\Omega_{0(f-1)} = \frac{1 - \Omega_{m0} - \Omega_{r0}}{2} \left(1 + \left(\frac{1 + z_{f-1}}{1 + z_f} \right)^{\alpha_{f-1}} \right), \quad (3.8)$$

and so on. In this way we can relate some of the parameters with others and reduce the number of parameters.

The EoS of the scalar field w_ϕ can be parameterized from Eq. (3.1) using the the continuity equation of the scalar field

$$\dot{\rho}_\phi + 3H\rho_\phi(1 + w_\phi) = 0, \quad (3.9)$$

and is given by

$$w_\phi(z) = -1 + \frac{w_1(z)}{3\rho_\phi(z)}. \quad (3.10)$$

where

$$w_1(z) = -\frac{\dot{\rho}_\phi}{H} = \sum_{i=1}^f \frac{\rho_{0i}\alpha_i \left(\frac{1+z_i}{1+z} \right)^{\alpha_i}}{\left(1 + \left(\frac{1+z_i}{1+z} \right)^{\alpha_i} \right)^2} + 6\rho_{\text{KE}}(1+z)^6, \quad (3.11)$$

4 Scaling-freezing dynamics

For scaling-freezing dynamics we consider the following double exponential potential [28, 40]

$$V(\phi) = V_1 e^{-\lambda_1 \phi/M_{\text{Pl}}} + V_2 e^{-\lambda_2 \phi/M_{\text{Pl}}}, \quad (4.1)$$

for which the corresponding

$$\Gamma = 1 - \frac{(\lambda - \lambda_1)(\lambda - \lambda_2)}{\lambda^2}, \quad (4.2)$$

where V_1 and V_2 are constant and they set the energy scales while λ_1 and λ_2 are the slopes of the two exponential functions and are constants too. This potential was introduced in [28] for $V_1 = V_2$. Now, considering $V_1 \neq V_2$ we can relate two energy scales dynamically by a scalar

field. Let's consider $V_1 > V_2$. Now, to get scaling solution the slope of the exponential function associated with V_1 should be $> \sqrt{3}$ *i.e.*, $\lambda_1 > \sqrt{3}$ [27]. In fact, fixed the point associated with the scaling solution tells us that $\Omega_\phi = 4/\lambda_1^2$ during radiation era and $\Omega_\phi = 3/\lambda_1^2$ during matter era [27]. Since Ω_ϕ should be very small during matter era we can say, to estimate, that $\Omega_\phi < 0.1$ which tells us that $\lambda_1 > \sqrt{30}$. So, by fixing $\lambda_1 > \sqrt{30}$ we can get scaling solutions and maintain scalar field energy density as the small fraction in total energy density during matter era. Now, the slope λ can vary between λ_1 and λ_2 . As long as $\lambda \approx \lambda_1$ we have scaling dynamics as, from Eq. (4.2), we see $\Gamma \approx 1$ for this case and we have considered large values of λ_1 . Once λ starts moving away from λ_1 the function Γ also starts moving away from 1 which results to the exit from the scaling behaviour in the scalar field dynamics. Eventually λ becomes same as λ_2 and Γ again becomes 1 but if we consider $\lambda_2 < \sqrt{3}$ then we don't have scaling solution rather we can have late time acceleration. So, to get late time acceleration we can fix V_2 at the dark energy scale with small value of $\lambda_2 < \sqrt{3}$. One should also note that, if we consider negative values of λ_2 then the potential (4.1) becomes an oscillatory potential which can also give rise to late time acceleration [41].

Considering that the scaling behaviour exists during the matter era then for scaling-freezing dynamics we can consider $f = 2$ and the parametrization (3.1) becomes

$$\rho_\phi(z) = \frac{\rho_{02}}{1 + \left(\frac{1+z_2}{1+z}\right)^{\alpha_2}} + \frac{\rho_{01}}{1 + \left(\frac{1+z_1}{1+z}\right)^{\alpha_1}} + \rho_{\text{KE}}(1+z)^6. \quad (4.3)$$

For this case Eq. (3.2) reduces to

$$1 + z_2 = \left(\frac{2\rho_{01}}{\rho_{02}} - 1\right)^{-1/\alpha_1} (1 + z_1) \quad (4.4)$$

and Eq. (3.7) reduces to (using $\Omega_{0i} = \rho_{0i}/\rho_{c0}$)

$$1 + z_2 = \left(\frac{\Omega_{02}}{1 - \Omega_{m0} - \Omega_{r0}} - 1\right)^{1/\alpha_2}. \quad (4.5)$$

From the last two equations we have

$$1 + z_1 = \left(\frac{\Omega_{02}}{1 - \Omega_{m0} - \Omega_{r0}} - 1\right)^{1/\alpha_2} \left(\frac{2\rho_{01}}{\rho_{02}} - 1\right)^{1/\alpha_1} \quad (4.6)$$

So, the extra parameters are Ω_{01} , Ω_{02} , α_1 and α_2 . ρ_{KE} sets the initial value of ρ_ϕ . $\rho_{\text{KE}} = 0$ implies that the scalar field is initially frozen *i.e.*, its kinetic term is almost zero. If $\rho_{\text{KE}} \neq 0$ then ρ_ϕ initially falls as a^{-6} and becomes subdominant which causes huge Hubble damping. Because of this Hubble damping the scalar field freezes to evolve. During the frozen period ρ_ϕ increases and becomes comparable to the background energy density and starts evolving again. This redshift from which the scalar field starts evolving again is denoted by z_1 and scalar field energy density at z_1 is associated with ρ_{01} . If the potential is very steep then ρ_ϕ may again fall as a^{-6} and repeat the previous dynamics. Since we have considered that the scalar field scales the matter we can safely choose $\alpha_1 = 4$. If the scaling behaviour starts from radiation era we have to consider $f = 3$. For $z_2 \leq z \leq z_1$ the scaling regime persists and for $z < z_2$ the scalar field starts deviating from the scaling regime. If we choose $\alpha_2 < 1$ the scalar field EoS will be closer to -1 at $z = 0$. The EoS of the scalar field follows from Eq. (3.10)

$$w_\phi(z) = -1 + \frac{1}{3\rho_\phi} \left(\frac{\rho_{02}\alpha_2 \left(\frac{1+z_2}{1+z}\right)^{\alpha_2}}{\left(1 + \left(\frac{1+z_2}{1+z}\right)^{\alpha_2}\right)^2} + \frac{\rho_{01}\alpha_1 \left(\frac{1+z_1}{1+z}\right)^{\alpha_1}}{\left(1 + \left(\frac{1+z_1}{1+z}\right)^{\alpha_1}\right)^2} + 6\rho_{\text{KE}}(1+z)^6 \right), \quad (4.7)$$

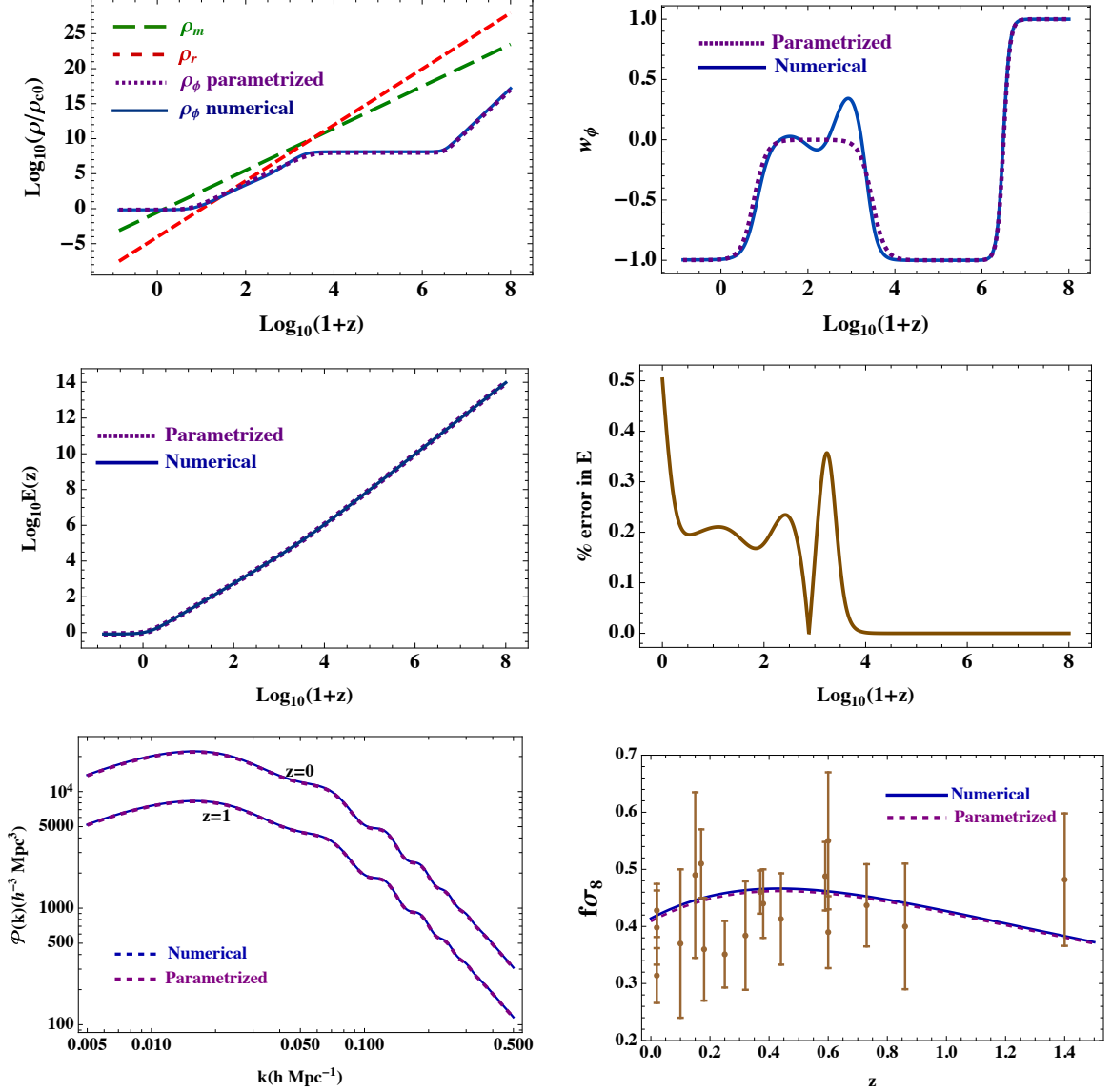


Figure 1. (Top left) Evolution of energy densities of matter (long dashed green), radiation (short dashed red) and scalar field (solid blue line is numerically evolved and dotted purple line is parametrized) normalised with the present value of critical density ρ_{c0} along with the numerically evolved and parametrized EoS of the scalar field (top right), normalised Hubble parameter $E(z)$ (middle left), the percentage error in $E(z)$ (middle right), (bottom left) matter power spectrum for $z = 0$ (upper) and $z = 1$ (lower) and (bottom right) evolution of $f\sigma_8$ along with the observational data and their error bars have been shown. In the bottom right figure the brown dots are the observational data of $f\sigma_8(z)$ along with their 1σ error bars [42]. For the numerical curves the initial conditions and parameter values are $V_1 = 10^9\rho_{c0}$, $V_2 = 0.79\rho_{c0}$, $\lambda_1 = 20$, $\lambda_2 = 0.1$, initial field value $\phi_i = 0.1M_{\text{Pl}}$ and $\phi'_i = d\phi_i/d\ln(1+z) = 10^{-5}M_{\text{Pl}}$. For the parametrized curves we have taken $\Omega_{\text{KE}} = 10^{-31}$, $\Omega_{01} = 10^8$, $\Omega_{02} = 1.4123$, $\alpha_1 = 3$ and $\alpha_2 = 0.01$.

Fig. 1 compares the numerical results with the parametrization (4.3) for the double exponential potential (4.1). We can see that the parametrization, represented by the dotted purple lines, mimics the numerical results, represented by solid blue lines. Around the redshift

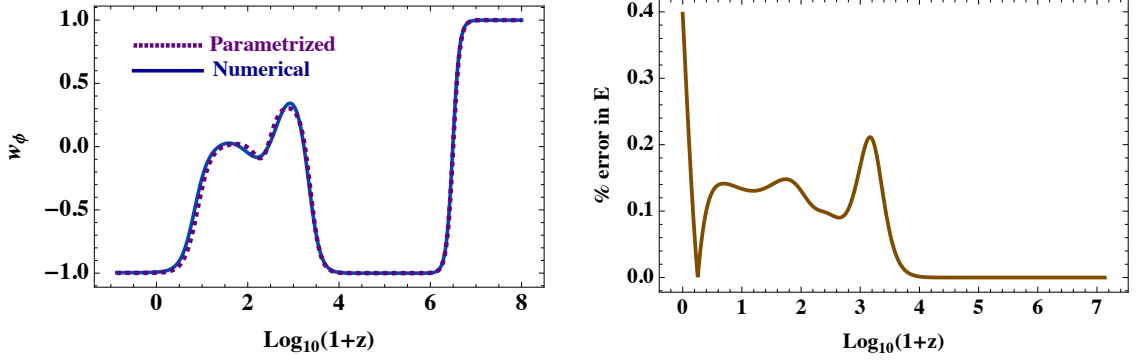


Figure 2. Evolution of scalar field EoS (left) and the percentage error in $E(z)$ has been shown. For the numerical curves the initial conditions and parameter values are $V_1 = 10^9 \rho_{c0}$, $V_2 = 0.79 \rho_{c0}$, $\lambda_1 = 20$, $\lambda_2 = 0.1$, initial field value $\phi_i = 0.1 M_{\text{Pl}}$ and $\phi'_i = d\phi_i/d\ln(1+z) = 10^{-5} M_{\text{Pl}}$. For the parametrized curves we have taken $\Omega_{\text{KE}} = 10^{-31}$, $\Omega_{01} = 10^8$, $\Omega_{02} = 1.3 \times 10^4$, $\Omega_{03} = 1.4145$, $\alpha_1 = 4$, $\alpha_2 = 3$ and $\alpha_3 = 0.01$.

range 100 to 1000 the parametrized EoS, given in Eq. (4.7) gives the average value of the numerically evolved EoS which has an oscillatory behaviour during that period (top right figure of Fig. 1). We can match this oscillatory behaviour by increasing one more value of f which we will show shortly. The evolution of the normalized Hubble parameter $E(z) = H(z)/H_0$ is same for both parametrized and numerically evolved cases (middle left figure of Fig. 1). The similarity in the evolution in $E(z)$ has been quantified in the middle right figure of Fig. 1 that shows the *percentage error in $E(z)$* $= \frac{|E_{\text{parametrized}}(z) - E_{\text{numerical}}(z)|}{E_{\text{numerical}}(z)} \times 100\%$ and the maximum error that we get is around 0.4%. This shows that the amount of mismatch we have in the evolution of w_ϕ does not have any effect on the evolution of $E(z)$ and therefore the parametrization should lead to observational predictions similar to the numerical results. The top and middle figures of Fig. 1 show the validity of the parametrization (4.3) at the background level. To check the consistency of the parametrization with the numerical results at the perturbation level we have shown the matter power spectrum and the evolution of $f\sigma_8(z)$ in the bottom left and bottom right figures of Fig. 1 respectively. We see that the parametrization (4.3) predicts the power spectrum and the evolution of $f\sigma_8(z)$ similar to the numerical results. So, Fig. 1 shows the validity of the parametrization (4.3) not only at the background cosmology level but also at the perturbation level.

As we already have mentioned that the mismatch in the evolution of w_ϕ in the numerical and parametrized results, during the redshift range 100 to 1000, can be reduced by considering $f = 3$ instead of considering $f = 2$. For $f = 3$ the parametrization becomes

$$\rho_\phi(z) = \frac{\rho_{03}}{1 + \left(\frac{1+z_3}{1+z}\right)^{\alpha_3}} + \frac{\rho_{02}}{1 + \left(\frac{1+z_2}{1+z}\right)^{\alpha_2}} + \frac{\rho_{01}}{1 + \left(\frac{1+z_1}{1+z}\right)^{\alpha_1}} + \rho_{\text{KE}} (1+z)^6, \quad (4.8)$$

and the relations between the parameters will be

$$1 + z_3 = \left(\frac{\Omega_{03}}{1 - \Omega_{\text{m}0} - \Omega_{\text{r}0}} - 1 \right)^{1/\alpha_3}. \quad (4.9)$$

$$1 + z_2 = \left(\frac{\Omega_{03}}{1 - \Omega_{\text{m}0} - \Omega_{\text{r}0}} - 1 \right)^{1/\alpha_3} \left(\frac{2\Omega_{02}}{\Omega_{03}} - 1 \right)^{1/\alpha_2}, \quad (4.10)$$

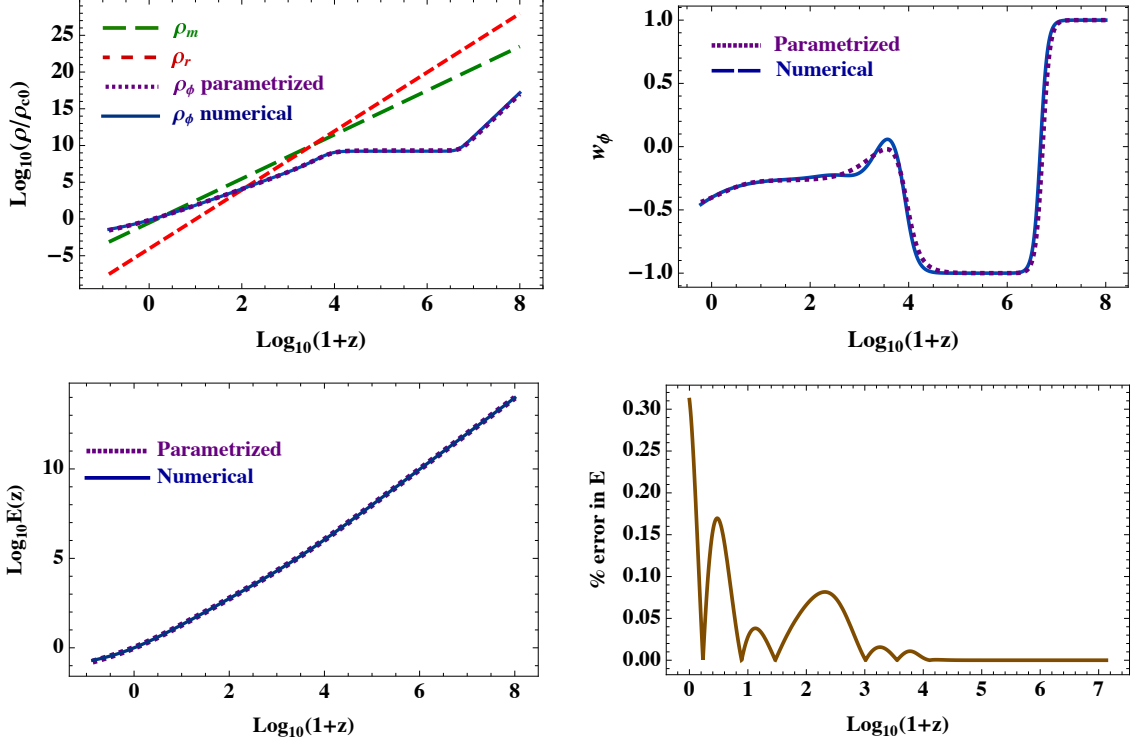


Figure 3. Figures represent the same cosmological parameters as the upper and middle figures of Fig. 1 for the potential (5.1) and parametrization (4.8). For the numerical curves the initial conditions and parameter values are $V_0 = 1700\rho_{c0}$, $n = 6$, initial field value $\phi_i = 0.1M_{\text{Pl}}$ and $\phi'_i = d\phi_i/d\ln(1+z) = 10^{-5}M_{\text{Pl}}$. For the parametrized curves we have taken $\Omega_{\text{KE}} = 10^{-31}$, $\Omega_{01} = 1.5 \times 10^9$, $\Omega_{02} = 5.7 \times 10^8$, $\Omega_{03} = 1.1$, $z_1 = 9000$, $\alpha_1 = 3.5$, $\alpha_2 = 2.2$ and $\alpha_3 = 1.3$.

$$1 + z_1 = \left(\frac{\Omega_{03}}{1 - \Omega_{m0} - \Omega_{r0}} - 1 \right)^{1/\alpha_3} \left(\frac{2\Omega_{02}}{\Omega_{03}} - 1 \right)^{1/\alpha_2} \left(\frac{2\Omega_{01}}{\Omega_{02}} - 1 \right)^{1/\alpha_1}. \quad (4.11)$$

As we choose $f = 3$ the parametrization almost mimics the evolution of w_ϕ which is shown in the left figure of Fig. 2. Although we have this improvement in the evolution of w_ϕ , it has almost no effect on the evolution of $E(z)$ which has been shown in the right figure of Fig. 2. So, we can say that the parametrization (4.3) is sufficient to mimic any scaling-freezing dynamics.

5 Tracker dynamics

For tracker dynamics we consider the inverse power law potential [24, 30]

$$V(\phi) = V_0 \left(\frac{M_{\text{Pl}}}{\phi} \right)^{-n} \quad (5.1)$$

and the inverse axionlike potential [33]

$$V(\phi) = V_0 \left(1 - \cos \left(\frac{\phi}{f_{\text{pl}}} \right) \right)^{-n}, \quad (5.2)$$

where, n , f_{pl} , V_0 are constants and $n > 0$. For $n < 0$ the potential (5.2) becomes the axionlike potential which is a well studied potential in cosmology [43–48]. In tracker dynamics, the

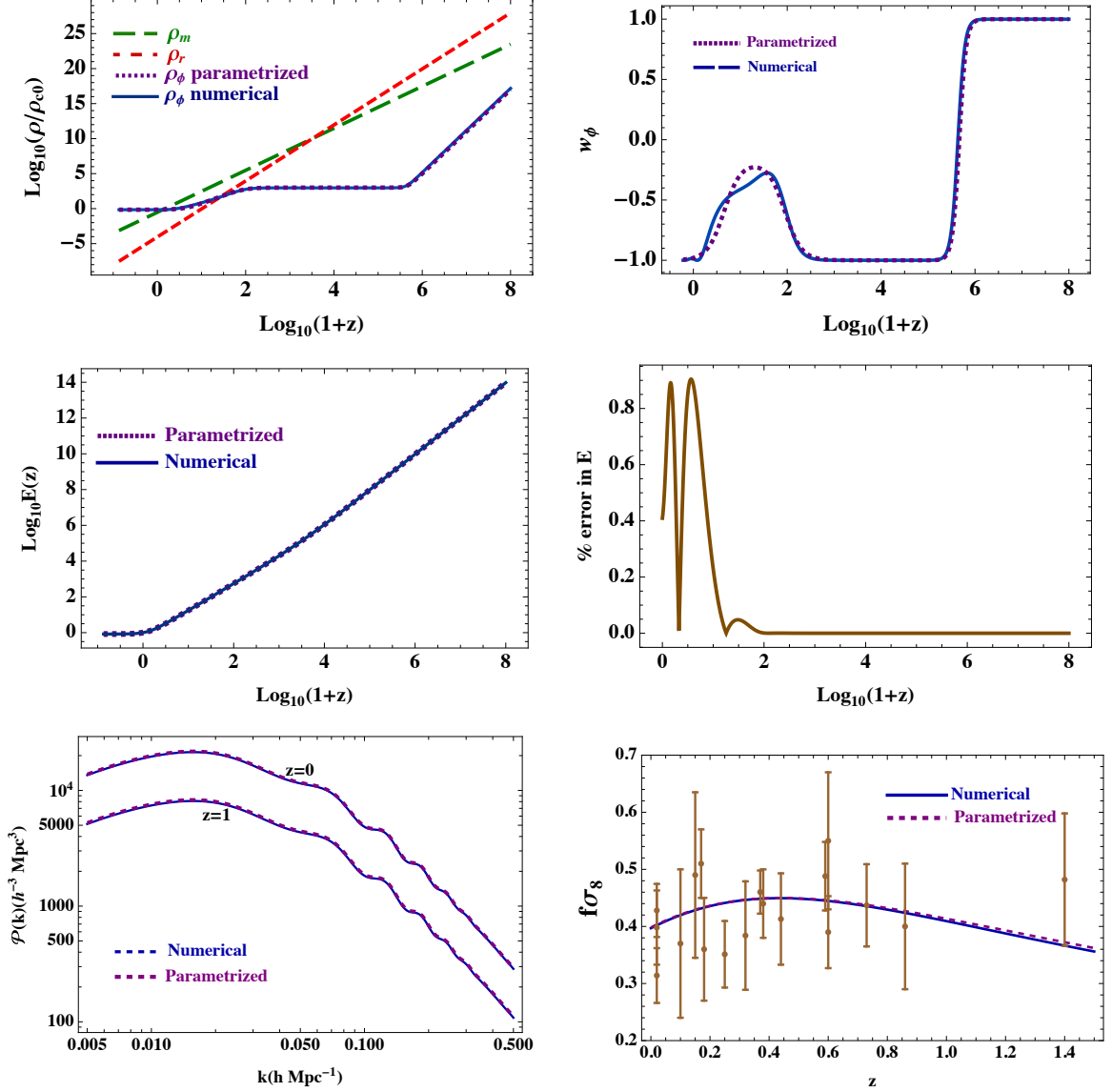


Figure 4. Curves represent the same cosmological parameters as Fig. 1 for the potential (5.2) and parametrization (4.3). For the numerical evolution we have considered $n = 2$ and the initial conditions are $\phi_i = 0.1M_{\text{Pl}}$ and $\phi'_i = d\phi_i/d\ln(1+z) = 10^{-5}M_{\text{Pl}}$. For the parametrized curves we have taken $\Omega_{\text{KE}} = 10^{-31}$, $\Omega_{01} = 10^3$, $z_1 = 88$ and $\alpha_1 = 2.44$.

scalar field energy density ρ_ϕ has a frozen period during early times. After the frozen period ρ_ϕ does not exactly follow the background and instead decays, at least during late times, a little slower than the background. Because of this nature the scalar field energy density takes over the matter but if the potential does not have necessary shallow region the kinetic energy of the scalar field may contribute significantly. This results in a much larger EoS than -1 . This happens for the inverse power potential (5.1) and we can't get viable cosmology in this case if we have tracker dynamics [30, 33]. This problem does not exist in the inverse axionlike potential (5.2) as the potential can generate a CC like term during the late time [33] which leads to a viable cosmology. This special feature of this potential also relates the dark energy

scale with any higher energy scale. In other words, we can generate CC like term from any higher energy scale by tuning the parameters of the potential [33].

Tracker dynamics can be parametrized with the parametrization (4.8). For the inverse power law potential (5.1), as we have significant contribution from kinetic energy, the constraint equation (3.6) changes to

$$\Omega_{m0} + \Omega_{r0} + \frac{\Omega_{0f}}{1 + (1 + z_f)^{\alpha_f}} + \frac{\Omega_{0(f-1)}}{1 + (1 + z_{f-1})^{\alpha_{f-1}}} = 1, \quad (5.3)$$

which, for the parametrization (4.8), becomes

$$\Omega_{m0} + \Omega_{r0} + \frac{\Omega_{03}}{1 + (1 + z_3)^{\alpha_3}} + \frac{\Omega_{02}}{1 + (1 + z_2)^{\alpha_2}} = 1, \quad (5.4)$$

From above equation we can represent z_3 in terms of the other parameters. Now, z_2 can be represented, following Eq. (3.2), as

$$1 + z_2 = \left(\frac{2\Omega_{01}}{\Omega_{02}} - 1 \right)^{-1/\alpha_1} (1 + z_1). \quad (5.5)$$

So, in this case we have to consider z_1 as a free parameter. Figs. 3 shows the comparison among the numerical results and parametrized results using the parametrization (4.8) for the inverse power law potential (5.1). We can see that the parametrization (4.8) mimics the tracker dynamics achieved numerically. The maximum difference in the evolution of the Hubble parameter is about 0.3%.

For the inverse axionlike potential (5.2) we can relate V_0 with the dark energy density as [33]

$$V_0 = 2^n (1 - \Omega_{m0} - \Omega_{r0}) \rho_{c0}, \quad (5.6)$$

i.e., we get a CC like term automatically in this potential during the late time. So, in this potential the dynamics around $z = 0$ is very similar to the standard Λ CDM model. Considering this we can choose $f = 2$ with $\alpha_2 = 0$. So, the parametrization can be

$$\rho_\phi(z) = \frac{\rho_{02}}{2} + \frac{\rho_{01}}{1 + \left(\frac{1+z_1}{1+z} \right)^{\alpha_1}} + \rho_{KE} (1+z)^6, \quad (5.7)$$

where $\rho_{02} = 2(1 - \Omega_{m0} - \Omega_{r0})$. If we fix ρ_{KE} then the free parameters are ρ_{01} , z_1 and α_1 . In Fig. 4 the comparison between the numerical and parametrized results has been shown in terms of different cosmological parameters. We can see that the parametrization (5.7) fits quiet well with the numerical results for both at the background and perturbation level.

6 Thawing dynamics

In thawing dynamics the scalar field remains frozen for most of the time and starts rolling down the potential from the recent past. So the dynamics is very similar to the standard Λ CDM except at the present time when the EoS can deviate from -1 . So, for thawing dynamics we can choose $f = 1$ and the parametrization of the scalar field energy density becomes

$$\rho_\phi(z) = \frac{\rho_{01}}{1 + \left(\frac{1+z_1}{1+z} \right)^{\alpha_1}} + \rho_{KE} (1+z)^6, \quad (6.1)$$

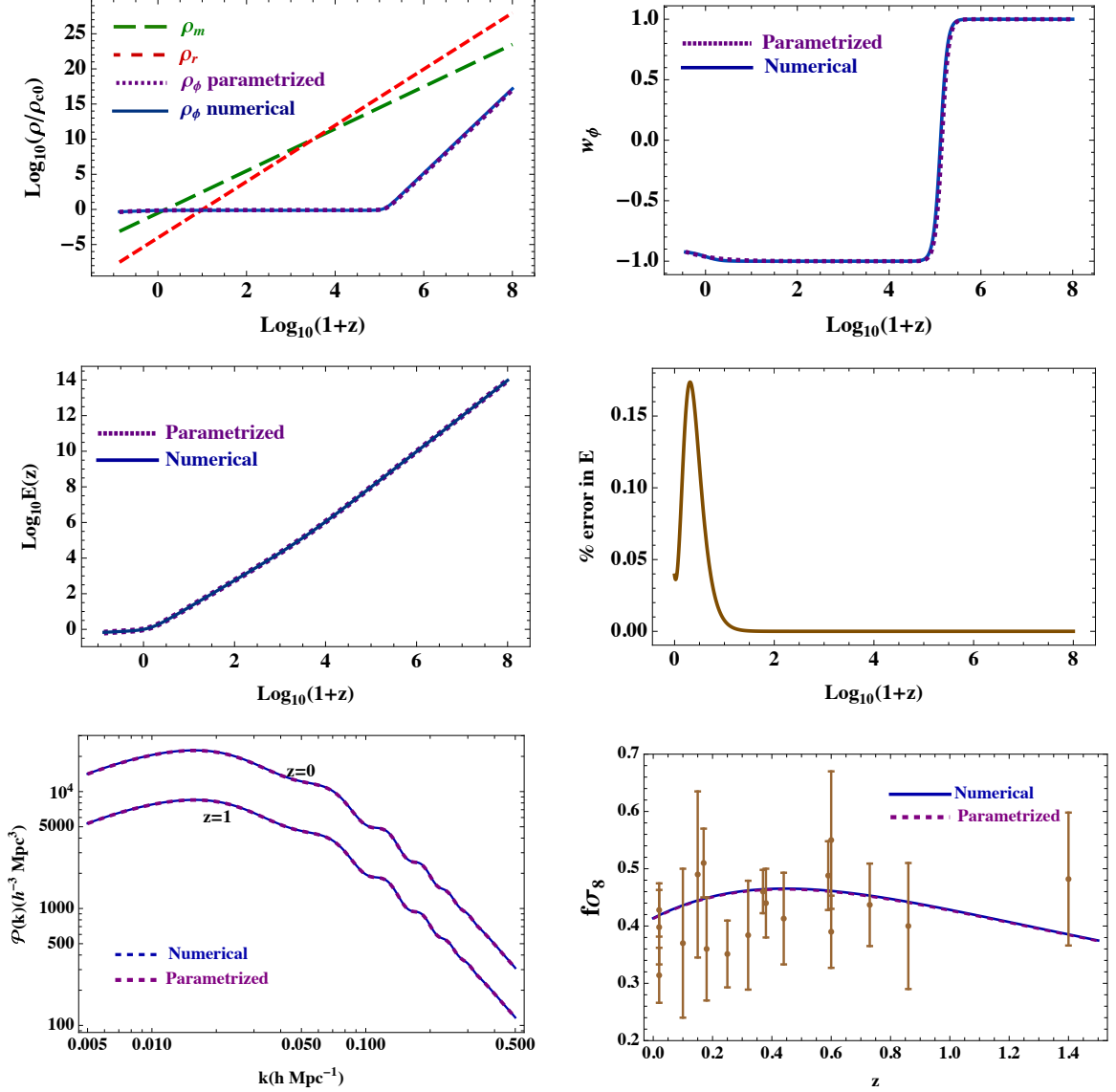


Figure 5. Similar figure as Fig. 1 have been shown for the potential (6.3). For the numerical curves the initial conditions and parameter values are $V_0 = 0.95\rho_{c0}$, $\beta = 0.5$, initial field value $\phi_i = 0.5M_{\text{Pl}}$ and $\phi'_i = d\phi_i/d\ln(1+z) = 10^{-5}M_{\text{Pl}}$. For the parametrized curves we have taken $\Omega_{\text{KE}} = 10^{-31}$, $\Omega_{01} = 0.8$, $\alpha_1 = 0.9$.

with

$$1 + z_1 = \left(\frac{\Omega_{01}}{1 - \Omega_{m0} - \Omega_{r0}} - 1 \right)^{1/\alpha_1}. \quad (6.2)$$

For the numerical purpose we consider an exponential potential of the following form

$$V(\phi) = V_0 e^{-\beta\phi/M_{\text{Pl}}}. \quad (6.3)$$

Fig. 5 compares the numerical results with the parametrization (6.1) for the exponential potential (6.3) for thawing dynamics. We can see that the parametrization mimics the

numerical results. The similarity in the evolution has been quantified in the lower right figure of Fig. 5 which shows the *percentage error in $E(z)$* and the maximum error that we are getting is around 0.15%. The lower figures of Fig. 5 shows the power spectrum (left) and the evolution of $f\sigma_8(z)$ (right) for both numerical and parametrized cases and we can see that the parametrized results mimic the numerical ones.

7 Observational Constraints

In this section we study the observational constraints on the standard Λ CDM model and models with the parametrization (3.1) with $f = 1$ and $f = 2$. We also compare these three models by calculating the Akaike information criterion (AIC) and Bayesian Information Criterion (BIC) [49–52] along with the minimum chi-squared (χ_{\min}^2) and reduced chi-squared ($\chi_{\text{red}}^2 = \chi_{\min}^2/\nu$), where $\nu = k - N$ is the degree of freedom while k and N are the total number of data points and the total number of model parameters respectively. AIC and BIC are defined as

$$\text{AIC} = 2N - 2 \ln \mathcal{L}_{\max} = 2N + \chi_{\min}^2, \quad (7.1)$$

$$\text{BIC} = N \ln K - 2 \ln \mathcal{L}_{\max} = N \ln K + \chi_{\min}^2, \quad (7.2)$$

where, \mathcal{L}_{\max} is the maximum likelihood. We also compute the difference in AIC (ΔAIC) and BIC (ΔBIC) between the parametrized models with $f = 1$ and $f = 2$ and Λ CDM model such that

$$\Delta\text{AIC} = \text{AIC}_{\text{para}} - \text{AIC}_{\Lambda\text{CDM}} \quad (7.3)$$

$$\Delta\text{BIC} = \text{BIC}_{\text{para}} - \text{BIC}_{\Lambda\text{CDM}}, \quad (7.4)$$

where, the subscript *para* stands for *parametrized*. ΔAIC and ΔBIC tell us about the preference of the model by the observational data in comparison to a reference model which, in this case, we have considered Λ CDM model which also has less number of free parameters than the parametrized models.

For Λ CDM model we have six parameters $\{\Omega_{\text{m}0}, h, \omega_{\text{b}}, r_{\text{d}}h, \sigma_8, M\}$, $\omega_{\text{b}} = \Omega_{\text{m}0}h^2$, r_{d} is the sound horizon at the decoupling and M is the absolute magnitude. We consider uniform priors of the parameters as

$$\{\Omega_{\text{m}0}, h, \omega_{\text{b}}, r_{\text{d}}h, \sigma_8, M\} \equiv \{[0.2, 0.5], [0.5, 0.8], [0.005, 0.05], [60, 140], [0.5, 1], [-22, -15]\}.$$

From Eq. (6.1) we can see that for the parametrized model with $f = 1$ we have two extra parameters, Ω_{01} and α_1 , along with other five parameters mentioned above for the Λ CDM model. Instead of considering Ω_{01} we consider $((\Omega_{01}/(1 - \Omega_{\text{m}0} - \Omega_{\text{r}0})) - 1) = \Omega_{\delta}$ as the model parameter. Keeping the same prior for the common five parameters we choose the priors of the two extra parameter as $\{\Omega_{\delta}, \alpha_1\} \equiv \{[0, 5], [0, 1]\}$. We call this model as *Pf1*. To incorporate the phantom region we also consider the prior $\{\Omega_{\delta}, \alpha_1\} \equiv \{[0, 5], [-1, 1]\}$ and we call this model as *Pf1 + Phantom*.

$f = 2$ corresponds to the parametrization (4.3). This parametrization can represent both scaling-freezing and tracker dynamics as depicted above. For this parametrization we have four extra parameter, Ω_{δ} , Ω_{01} , α_2 and α_1 . We consider the following prior for these

parameters, $\{\Omega_\delta, \Omega_{01}, \alpha_2, \alpha_1\} \equiv \{[1.05, 1.8], [0, 14], [0.001, 0.12], [0.01, 3.5]\}$. We call this model as *Pf2*.

We perform Markov Chain Monte Carlo (MCMC) analysis to constrain the model parameters. We use the publicly available code **EMCEE** [53] for the purpose of MCMC simulation. For analysing the results and plotting the contours of the model parameters we use another publicly available python package **GetDist** [54]. For assessing chain convergence, we consider the Gelman-Rubin statistic [55] according to which the chains are converged when $|R - 1| \lesssim 0.01$.

7.1 Observational data

We consider the data from the observations of cosmic microwave background (CMB) radiation, baryon acoustic oscillation (BAO), type-Ia supernovae (SNeIa) and redshift space distortion (RSD).

7.1.1 CMB

The CMB distance prior uses the positions of the acoustic peak to determine the cosmological distance at the fundamental level. This prior is commonly incorporated using the following key parameters: shift parameter(R), acoustic scale (l_A), the baryon energy density (ω_b), spectral index(n_s). We use these distance priors reconstructed from the Planck TT,TE,EE+lowE data of 2018 [5] and given in [56].

7.1.2 BAO data from DESI DR1

In DESI DR1 BAO measurements [12, 57, 58] we have the measurements from the galaxy, quasar and Lyman- α forest tracers within the redshift range $0.1 < z < 4.2$. These include the bright galaxy sample (BGS) within the redshift range $0.1 < z < 0.4$, luminous red galaxy sample (LRG) in the redshift range $0.4 < z < 0.6$ and $0.6 < z < 0.8$, emission line galaxy sample (ELG) in $1.1 < z < 1.6$, combined LRG and ELG sample in $0.8 < z < 1.1$, the quasar sample (QSO) in $0.8 < z < 2.1$ [57] and the Lyman- α Forest Sample (Ly- α) in $1.77 < z < 4.16$ [58].

7.1.3 Type-Ia Supernova

We consider the distance moduli measurements from the PantheonPlus (PP) sample of Type-Ia supernovae (SNeIa), which consists of 1550 SNeIa luminosity distance measurements within the redshift range $0.001 < z < 2.26$ [59, 60].

7.1.4 Observational Hubble Data

We analyse observational data for the Hubble parameter measured at various redshifts within the redshift range of 0.07 to 1.965. We focus on a collection of 31 $H(z)$ measurements derived using the cosmic chronometric method [61].

7.1.5 Redshift Space Distortion

We consider the redshift space distortion (RSD) measurements of the cosmological growth rate, $f\sigma_8(z)$, from different surveys compiled in [42]. $f(a)$ is the growth factor and defined as

$$f(a) = \frac{d \ln \delta(a)}{d \ln a}, \quad (7.5)$$

where, $\delta(a)$ is the matter density contrast, $\delta\rho_m/\rho_m$, $\delta\rho_m$ being the matter density fluctuation of the background matter density ρ_m and $\sigma_8(z)$ is the root mean square amplitude of mass fluctuations within spheres of radius $8h^{-1}\text{Mpc}$ and given by

$$\sigma_8(z) = \sigma_8 \frac{\delta(z)}{\delta(0)}, \quad (7.6)$$

where, σ_8 is the present value of $\sigma_8(z)$, *i.e.*, $\sigma_8(0)$. We follow [42] to construct the covariance matrix and define the χ^2 for the RSD data. In this regard, it should be noted that the RSD data, from different measurements, have a dependence on the fiducial model used by the collaborations to convert redshifts to distances. To correct this we have to define a ratio

$$\text{ratio}(z) = \frac{H(z)D_A(z)}{H_{\text{fid}}(z)D_{A,\text{fid}}(z)} \quad (7.7)$$

where subscript *fid* stands for *fiducial* and the angular diameter distance $D_A(z) = (c/H_0)d_A(z)$, where $d_A(z) = (1/(1+z)) \int dz/E(z)$ with $E(z)$ being the dimensionless Hubble parameter, $H(z)/H_0$. The product $H(z)D_A(z)$ can be written as $E(z)d_A(z)$. Once we define the ratio (7.7) we can define the χ^2 as

$$\chi_{\text{RSD}}^2 = V^i C_{ij}^{-1} V^j, \quad (7.8)$$

where, the vector $V^i(z_i, \theta)$ is given by

$$V^i(z_i, \theta) = f\sigma_{8,i} - \text{ratio}(z_i)f\sigma_8(z_i, \theta), \quad (7.9)$$

where, $f\sigma_{8,i}$ is the value of the i th data point at the redshift z_i . θ represents the model parameters. C_{ij} is the covariance matrix which is an $N \times N$ diagonal matrix except at the positions of WiggleZ data as except the data from WiggleZ the other data are not correlated. So the covariance matrix can be written as

$$C_{ij} = \begin{pmatrix} \sigma_1^2 & 0 & 0 & \cdots & 0 \\ 0 & \sigma_2^2 & 0 & \cdots & 0 \\ \vdots & & \ddots & & \vdots \\ 0 & \cdots & C_{ij}^{\text{WiggleZ}} & \cdots & 0 \\ \vdots & \cdots & & \cdots & \vdots \\ 0 & \cdots & & \cdots & 0 \end{pmatrix}, \quad (7.10)$$

where, C_{ij}^{WiggleZ} is the covariance matrix of the WiggleZ measurements which is given by

$$C_{ij}^{\text{WiggleZ}} = 10^{-3} \begin{pmatrix} 6.400 & 2.570 & 0.000 \\ 2.570 & 3.969 & 2.540 \\ 0.000 & 2.540 & 5.184 \end{pmatrix}. \quad (7.11)$$

7.2 Results

We present the results of the cosmological data analysis for the data combination CMB + BAO + PP + Hubble + RSD in Tab. 1. From the values of ΔAIC and ΔBIC we can say the considered data prefers the standard ΛCDM model over the other three models. For the parametrization with $f = 2$, *i.e.*, $Pf2$ we see that the parameter Ω_{01} is unconstrained and

Table 1. Observational constraints of the parameters for Λ CDM, $Pf1$, $Pf1 + Phantom$ and $Pf2$ models are given along with the corresponding model comparison statistics with AIC and BIC.

Parameter	Λ CDM	$Pf1$	$Pf1 + Phantom$	$Pf2$
Ω_{m0}	0.3129 ± 0.0067	$0.3167^{+0.0068}_{-0.0077}$	0.3148 ± 0.0077	$0.3150^{+0.0065}_{-0.0076}$
h	0.6757 ± 0.0051	$0.6706^{+0.0067}_{-0.0056}$	0.6734 ± 0.0071	$0.6729^{+0.0060}_{-0.0052}$
ω_b	0.02240 ± 0.00014	0.02244 ± 0.00014	0.2242 ± 0.00014	0.02242 ± 0.00015
$r_d h$	100.46 ± 0.70	$99.71^{+0.91}_{-0.78}$	100.1 ± 1.0	$100.03^{+0.82}_{-0.72}$
σ_8	0.746 ± 0.029	0.744 ± 0.028	0.744 ± 0.029	0.743 ± 0.029
Ω_δ	---	< 2.72	< 2.66	> 1.37
Ω_{01}	---	---	---	unconstrained
α_{02}	---	---	---	< 0.07
α_{01}	---	< 0.208	$0.09^{+0.15}_{-0.22}$	> 1.53
M	-19.434 ± 0.015	$-19.445^{+0.017}_{-0.016}$	-19.439 ± 0.018	-19.439 ± 0.015
χ^2_{\min}	1447.00	1487.20	1446.94	1446.88
χ^2_{red}	0.90	0.90	0.88	0.88
AIC	1459.01	1503.19	1462.94	1466.88
Δ AIC	0	44.18	3.93	7.87
BIC	1491.40	1546.48	1506.23	1521.07
Δ BIC	0	55.08	14.83	29.67

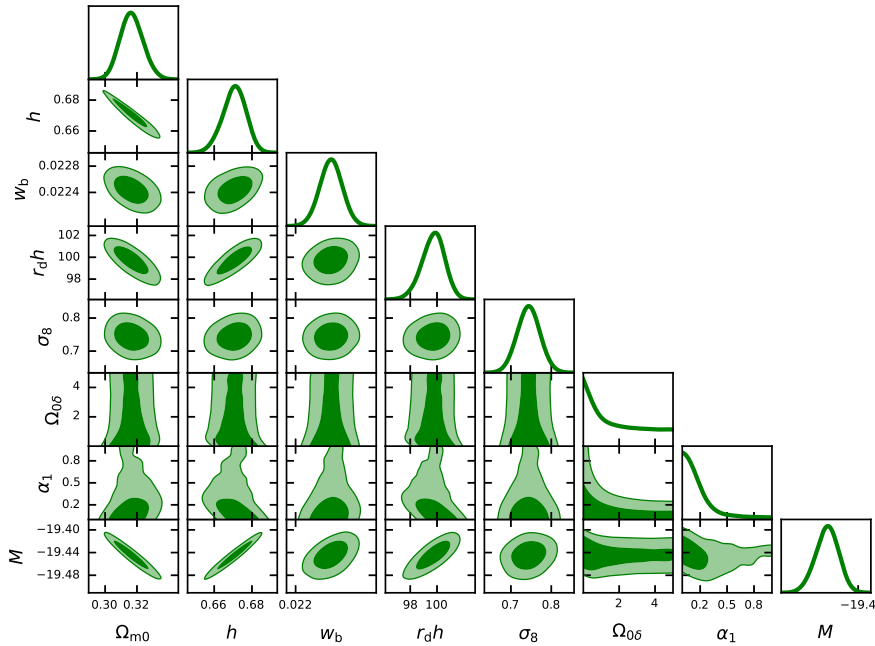


Figure 6. 1σ and 2σ confidence levels of the model parameters for the $Pf1$ model.

the parameters Ω_δ , α_{01} and α_{02} have bounds but the data can't fully constrain them. We hope in future we will be able to constrain these parameters with more precise data. In the

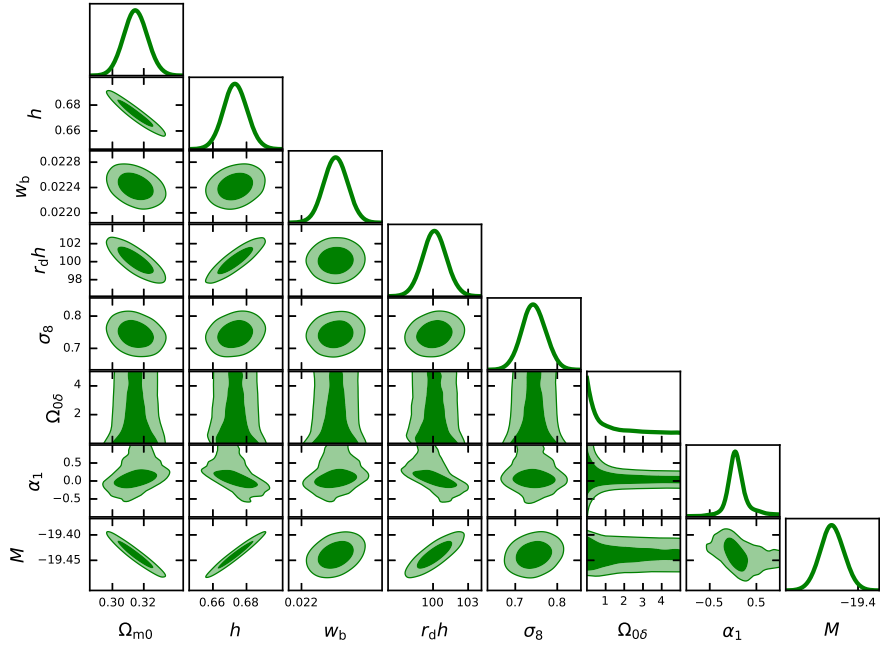


Figure 7. 1σ and 2σ confidence levels of the model parameters for the $Pf1 + Phantom$ model.

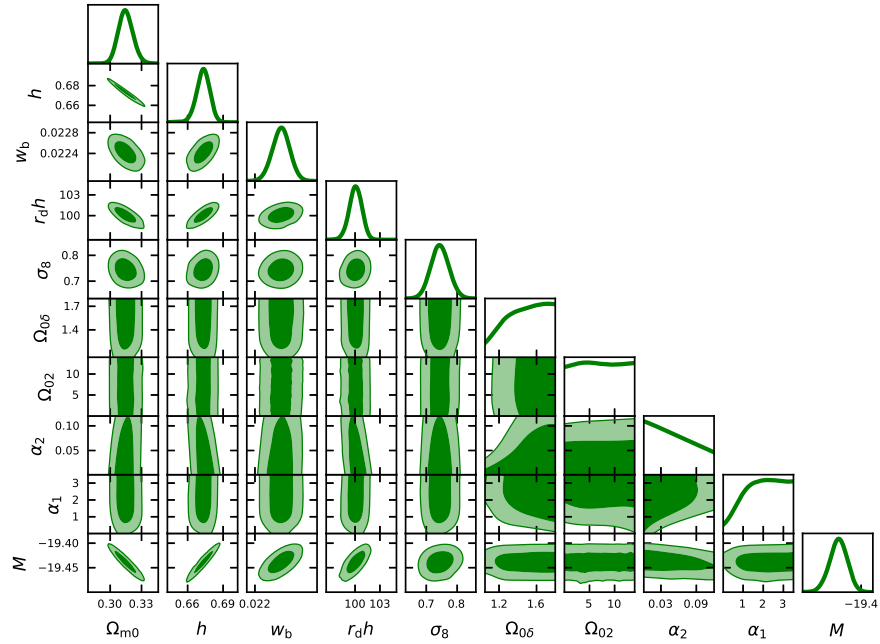


Figure 8. 1σ and 2σ confidence levels of the model parameters for the $Pf2$ model.

model $Pf1 + Phantom$ we consider the prior of α_{01} as $\{-1, 1\}$ to incorporate the phantom region. If we compare this model with the $Pf1$ model then it is very clear that the model $Pf1 + Phantom$ is significantly more preferred by the considered data compared to $Pf1$ as the values of ΔAIC and ΔBIC are less for the $Pf1 + Phantom$ model. Here we should mention

that the parametrization (3.1) is mainly for quintessence field. So, while considering the value of $\alpha_{01} < 0$ for $f = 1$ case can lead to phantom behaviour but the proper investigation should be done while using the parametrization (3.1). So basically if we consider thawing kind of dynamics then, we see, that the data prefers to have phantom region within 1σ bound. It is also interesting that the $f = 2$ case *i.e.*, $Pf2$, is more favoured by the data than $Pf1$ without the phantom region. We have not considered the phantom region for $Pf2$ as that has to be investigated properly first for the higher redshifts. This has to be noted that even after considering phantom region for $Pf1$ case the $\alpha_{01} = 0$, which represents a constant energy density or CC, is well within the 1σ bound. The contours of the parameters for the models $Pf1$, $Pf1 + Phantom$ and $Pf2$ are shown in the Figs. 6, 7 and 8 respectively.

8 Discussions and Conclusions

In this paper, we present a general parametrization (3.1) for the energy density of the quintessence field. This can also work as a parametrization for phantom scalar fields if we do not consider much higher redshifts. For higher redshifts it has to be investigated properly for the phantom cases. The parametrization (3.1) can successfully mimic all kind of scalar field dynamics, namely scaling-freezing, tracker and thawing dynamics which has been shown in the Secs. 4, 5 and 6 respectively. So, our parametrization can mimic the dynamics of a quintessence field for a particular potential as well as it can also behave as model-agnostic approach to work with scalar field models. Now, while it is interesting that the parametrization (3.1) can mimic any kind of quintessence dynamics it also needs more parameters to represent more complicated dynamics like scaling-freezing or tracker. Having more free parameters makes the scenario less interesting from the cosmological data analysis point of view as the current data may not be able to constrain all the parameters properly which can be seen in Fig. 8. But we expect that in near future we will have much more precise data and we will be able to constrain more free parameters. If we can do that then our parametrization will properly point towards the actual dynamics. Apart from this issue the main advantage of our parametrization is that it can mimic the actual dynamics of a quintessence field for a particular potential and it reduces the computing time for data analysis to a very significant amount. When we work with scalar fields the computation for data analysis is, in general, very time consuming. In this regard, the parametrization (3.1) can make it much more affordable computationally.

We have compared our scenario with the standard Λ CDM model using the recent cosmological data. In this regard we have considered $f = 1$ and $f = 2$. For $f = 1$ case we have considered both non-phantom ($Pf1$) and phantom ($Pf1 + Phantom$) regions. For $f = 2$ ($Pf2$) we have considered only non-phantom regions. Our results tell us that the cosmological data prefers Λ CDM model over other models. In fact, even though we have considered the DESI 2024 DR1 data of BAO the CC is well within the 1σ bound. Interestingly, the scenario $Pf1$, which is non-phantom consideration with thawing dynamics, is less preferred over the $Pf1 + Phantom$ which is with the phantom region. As expected, the parameter of $Pf2$ are less constraint.

Acknowledgments

MWH acknowledges the High Performance Computing facility Pegasus at IUCAA, Pune, India, for providing computing facilities. The authors acknowledge the financial support from

References

- [1] PLANCK collaboration, *Planck 2013 results. XVI. Cosmological parameters*, *Astron. Astrophys.* **571** (2014) A16 [[1303.5076](#)].
- [2] E.J. Copeland, M. Sami and S. Tsujikawa, *Dynamics of dark energy*, *Int. J. Mod. Phys. D* **15** (2006) 1753 [[hep-th/0603057](#)].
- [3] S. Bahamonde, C.G. Böhrer, S. Carloni, E.J. Copeland, W. Fang and N. Tamanini, *Dynamical systems applied to cosmology: dark energy and modified gravity*, *Phys. Rept.* **775-777** (2018) 1 [[1712.03107](#)].
- [4] A.G. Riess et al., *A Comprehensive Measurement of the Local Value of the Hubble Constant with $1 \text{ km s}^{-1} \text{ Mpc}^{-1}$ Uncertainty from the Hubble Space Telescope and the SH0ES Team*, *Astrophys. J. Lett.* **934** (2022) L7 [[2112.04510](#)].
- [5] PLANCK collaboration, *Planck 2018 results. VI. Cosmological parameters*, *Astron. Astrophys.* **641** (2020) A6 [[1807.06209](#)].
- [6] M. Kamionkowski and A.G. Riess, *The Hubble Tension and Early Dark Energy*, *Ann. Rev. Nucl. Part. Sci.* **73** (2023) 153 [[2211.04492](#)].
- [7] W.L. Freedman and B.F. Madore, *Progress in Direct Measurements of the Hubble Constant*, **2309.05618**.
- [8] J.L. Bernal, L. Verde and A.G. Riess, *The trouble with H_0* , *JCAP* **10** (2016) 019 [[1607.05617](#)].
- [9] L. Knox and M. Millea, *Hubble constant hunter's guide*, *Phys. Rev. D* **101** (2020) 043533 [[1908.03663](#)].
- [10] L. Perivolaropoulos and F. Skara, *Challenges for Λ CDM: An update*, *New Astron. Rev.* **95** (2022) 101659 [[2105.05208](#)].
- [11] KILO-DEGREE SURVEY, DARK ENERGY SURVEY collaboration, *DES Y3 + KiDS-1000: Consistent cosmology combining cosmic shear surveys*, *Open J. Astrophys.* **6** (2023) 2305.17173 [[2305.17173](#)].
- [12] DESI collaboration, *DESI 2024 VI: Cosmological Constraints from the Measurements of Baryon Acoustic Oscillations*, **2404.03002**.
- [13] DESI collaboration, *DESI 2024: Reconstructing Dark Energy using Crossing Statistics with DESI DR1 BAO data*, **2405.04216**.
- [14] W. Giarè, M.A. Sabogal, R.C. Nunes and E. Di Valentino, *Interacting Dark Energy after DESI Baryon Acoustic Oscillation measurements*, **2404.15232**.
- [15] K.V. Berghaus, J.A. Kable and V. Miranda, *Quantifying Scalar Field Dynamics with DESI 2024 Y1 BAO measurements*, **2404.14341**.
- [16] F.J. Qu, K.M. Surrao, B. Bolliet, J.C. Hill, B.D. Sherwin and H.T. Jense, *Accelerated inference on accelerated cosmic expansion: New constraints on axion-like early dark energy with DESI BAO and ACT DR6 CMB lensing*, **2404.16805**.
- [17] H. Wang and Y.-S. Piao, *Dark energy in light of recent DESI BAO and Hubble tension*, **2404.18579**.
- [18] W. Giarè, M. Najafi, S. Pan, E. Di Valentino and J.T. Firouzjaee, *Robust Preference for Dynamical Dark Energy in DESI BAO and SN Measurements*, **2407.16689**.
- [19] D. Shlivko and P.J. Steinhardt, *Assessing observational constraints on dark energy*, *Phys. Lett. B* **855** (2024) 138826 [[2405.03933](#)].

- [20] G. Ye, M. Martinelli, B. Hu and A. Silvestri, *Non-minimally coupled gravity as a physically viable fit to DESI 2024 BAO*, [2407.15832](#).
- [21] O.F. Ramadan, J. Sakstein and D. Rubin, *DESI Constraints on Exponential Quintessence*, [2405.18747](#).
- [22] J.-Q. Jiang, D. Pedrotti, S.S. da Costa and S. Vagnozzi, *Non-parametric late-time expansion history reconstruction and implications for the Hubble tension in light of DESI*, [2408.02365](#).
- [23] G. Payeur, E. McDonough and R. Brandenberger, *Do Observations Prefer Thawing Quintessence?*, [2411.13637](#).
- [24] B. Ratra and P.J.E. Peebles, *Cosmological Consequences of a Rolling Homogeneous Scalar Field*, *Phys. Rev. D* **37** (1988) 3406.
- [25] C. Wetterich, *Cosmologies With Variable Newton's 'Constant'*, *Nucl. Phys. B* **302** (1988) 645.
- [26] C. Wetterich, *Cosmology and the Fate of Dilatation Symmetry*, *Nucl. Phys. B* **302** (1988) 668 [[1711.03844](#)].
- [27] E.J. Copeland, A.R. Liddle and D. Wands, *Exponential potentials and cosmological scaling solutions*, *Phys. Rev. D* **57** (1998) 4686 [[gr-qc/9711068](#)].
- [28] T. Barreiro, E.J. Copeland and N.J. Nunes, *Quintessence arising from exponential potentials*, *Phys. Rev. D* **61** (2000) 127301 [[astro-ph/9910214](#)].
- [29] V. Sahni and L.-M. Wang, *A New cosmological model of quintessence and dark matter*, *Phys. Rev. D* **62** (2000) 103517 [[astro-ph/9910097](#)].
- [30] P.J. Steinhardt, L.-M. Wang and I. Zlatev, *Cosmological tracking solutions*, *Phys. Rev. D* **59** (1999) 123504 [[astro-ph/9812313](#)].
- [31] I. Zlatev, L.-M. Wang and P.J. Steinhardt, *Quintessence, cosmic coincidence, and the cosmological constant*, *Phys. Rev. Lett.* **82** (1999) 896 [[astro-ph/9807002](#)].
- [32] R.J. Scherrer and A.A. Sen, *Thawing quintessence with a nearly flat potential*, *Phys. Rev. D* **77** (2008) 083515 [[0712.3450](#)].
- [33] M.W. Hossain and A. Maqsood, *A comparison between axion-like and power law potentials in cosmological background*, [2311.17825](#).
- [34] M. Chevallier and D. Polarski, *Accelerating universes with scaling dark matter*, *Int. J. Mod. Phys. D* **10** (2001) 213 [[gr-qc/0009008](#)].
- [35] E.V. Linder, *Exploring the expansion history of the universe*, *Phys. Rev. Lett.* **90** (2003) 091301 [[astro-ph/0208512](#)].
- [36] G. Efstathiou, *Constraining the equation of state of the universe from distant type Ia supernovae and cosmic microwave background anisotropies*, *Mon. Not. Roy. Astron. Soc.* **310** (1999) 842 [[astro-ph/9904356](#)].
- [37] H.K. Jassal, J.S. Bagla and T. Padmanabhan, *Observational constraints on low redshift evolution of dark energy: How consistent are different observations?*, *Phys. Rev. D* **72** (2005) 103503 [[astro-ph/0506748](#)].
- [38] E.M. Barboza, Jr. and J.S. Alcaniz, *A parametric model for dark energy*, *Phys. Lett. B* **666** (2008) 415 [[0805.1713](#)].
- [39] R.R. Caldwell and E.V. Linder, *The Limits of quintessence*, *Phys. Rev. Lett.* **95** (2005) 141301 [[astro-ph/0505494](#)].
- [40] L. Jarv, T. Mohaupt and F. Saueressig, *Quintessence cosmologies with a double exponential potential*, *JCAP* **08** (2004) 016 [[hep-th/0403063](#)].
- [41] M.S. Turner, *Coherent Scalar Field Oscillations in an Expanding Universe*, *Phys. Rev. D* **28** (1983) 1243.

- [42] S. Nesseris, G. Pantazis and L. Perivolaropoulos, *Tension and constraints on modified gravity parametrizations of $G_{\text{eff}}(z)$ from growth rate and Planck data*, *Phys. Rev. D* **96** (2017) 023542 [[1703.10538](#)].
- [43] D.J.E. Marsh, *Axion Cosmology*, *Phys. Rept.* **643** (2016) 1 [[1510.07633](#)].
- [44] V. Poulin, T.L. Smith, T. Karwal and M. Kamionkowski, *Early Dark Energy Can Resolve The Hubble Tension*, *Phys. Rev. Lett.* **122** (2019) 221301 [[1811.04083](#)].
- [45] V. Poulin, T.L. Smith, D. Grin, T. Karwal and M. Kamionkowski, *Cosmological implications of ultralight axionlike fields*, *Phys. Rev. D* **98** (2018) 083525 [[1806.10608](#)].
- [46] V. Poulin, T.L. Smith and T. Karwal, *The Ups and Downs of Early Dark Energy solutions to the Hubble tension: A review of models, hints and constraints circa 2023*, *Phys. Dark Univ.* **42** (2023) 101348 [[2302.09032](#)].
- [47] T.L. Smith, V. Poulin and M.A. Amin, *Oscillating scalar fields and the Hubble tension: a resolution with novel signatures*, *Phys. Rev. D* **101** (2020) 063523 [[1908.06995](#)].
- [48] R. Hlozek, D. Grin, D.J.E. Marsh and P.G. Ferreira, *A search for ultralight axions using precision cosmological data*, *Phys. Rev. D* **91** (2015) 103512 [[1410.2896](#)].
- [49] H. Akaike, *A New Look at the Statistical Model Identification*, *IEEE Transactions on Automatic Control* **19** (1974) 716.
- [50] A.R. Liddle, P. Mukherjee and D. Parkinson, *Cosmological model selection*, [astro-ph/0608184](#).
- [51] R. Trotta, *Bayesian Methods in Cosmology*, [1701.01467](#).
- [52] K. Shi, Y. Huang and T. Lu, *A comprehensive comparison of cosmological models from latest observational data*, *Mon. Not. Roy. Astron. Soc.* **426** (2012) 2452 [[1207.5875](#)].
- [53] D. Foreman-Mackey, D.W. Hogg, D. Lang and J. Goodman, *emcee: The MCMC Hammer*, *Publ. Astron. Soc. Pac.* **125** (2013) 306 [[1202.3665](#)].
- [54] A. Lewis, *GetDist: a Python package for analysing Monte Carlo samples*, [1910.13970](#).
- [55] A. Gelman and D.B. Rubin, *Inference from Iterative Simulation Using Multiple Sequences*, *Statist. Sci.* **7** (1992) 457.
- [56] L. Chen, Q.-G. Huang and K. Wang, *Distance priors from Planck final release*, *JCAP* **2019** (2019) 028 [[1808.05724](#)].
- [57] DESI collaboration, *DESI 2024 III: Baryon Acoustic Oscillations from Galaxies and Quasars*, [2404.03000](#).
- [58] DESI collaboration, *DESI 2024 IV: Baryon Acoustic Oscillations from the Lyman Alpha Forest*, [2404.03001](#).
- [59] D. Scolnic et al., *The Pantheon+ Analysis: The Full Data Set and Light-curve Release*, *Astrophys. J.* **938** (2022) 113 [[2112.03863](#)].
- [60] D. Brout et al., *The Pantheon+ Analysis: Cosmological Constraints*, *Astrophys. J.* **938** (2022) 110 [[2202.04077](#)].
- [61] A. Gómez-Valent and L. Amendola, *H_0 from cosmic chronometers and Type Ia supernovae, with Gaussian Processes and the novel Weighted Polynomial Regression method*, *JCAP* **2018** (2018) 051 [[1802.01505](#)].